Cardiovascular Diabetology

RESEARCH

Open Access

Mural cell dysfunction contributes to diastolic heart failure by promoting endothelial dysfunction and vessel remodelling

Mandy O. J. Grootaert[1,2*], Alessandra Pasut[3], Jana Raman[1], Steven J. Simmonds[1], Bram Callewaert[1], Ümare Col[1], Mieke Dewerchin[3,4], Peter Carmeliet[3,4], Stephane Heymans[1,5†] and Elizabeth A. V. Jones[1,5*†]

Abstract

Background Heart failure with preserved ejection fraction (HFpEF) is a complex cardiovascular disease associated with metabolic comorbidities. Microvascular dysfunction has been proposed to drive HFpEF, likely via endothelial cell (EC) dysfunction, yet the role of the mural cells herein has never been explored.

Methods We used the diabetic db/db mouse given 1% salt as a new model of HFpEF and crossed then with PDGFRβ$^{tg/tg}$-CreERT2-EYFP$^{tg/tg}$ mice to label the mural cells. We combined single-cell RNA sequencing, NichetNet analysis and histology to determine the role of mural cell dysfunction in HFpEF.

Results Db/db mice given 1% salt for 8 weeks developed diastolic dysfunction preceded by capillary density loss, pericyte loss and vessel regression. At 4 weeks of salt, hearts of db/db mice already showed EC dysfunction associated with an anti-angiogenic signature, and an increase in pericyte-EC intracellular space. Db/db + salt hearts were further characterised by increased ACTA2 expression, arteriole wall thickening and vessel enlargement. NicheNet analysis on the single cell transcriptomic data revealed little signalling from the ECs to the mural cells; instead, mural cells signalled strongly to ECs. Mechanistically, pericyte dysfunction induces an EC growth arrest via TNFα-dependent paracrine signalling and downstream signalling through STAT1.

Conclusion Mural cell dysfunction contributes to HFpEF by inducing coronary vessel remodelling, at least in part by reducing EC proliferation and inducing EC inflammation through TNFα-dependent paracrine signalling.

Background

Heart failure with preserved ejection fraction (HFpEF) is a chronic, progressive cardiovascular disease affecting more than half of all heart failure patients [1]. HFpEF is characterised by diastolic dysfunction, cardiomyocyte hypertrophy, cardiac inflammation and fibrosis, and is strongly associated with renal dysfunction and metabolic comorbidities such as type 2 diabetes, obesity and hypertension [2]. Despite its increasing prevalence, the pathophysiology of HFpEF is poorly understood. Microvascular dysfunction is an important determinant in HFpEF [3] and refers to any structural or functional

†Stephane Heymans and Elizabeth A. V. Jones have contributed equally to this work.

*Correspondence:
Mandy O. J. Grootaert
mandy.grootaert@kuleuven.be
Elizabeth A. V. Jones
liz.jones@kuleuven.be

Full list of author information is available at the end of the article

Graphic abstract

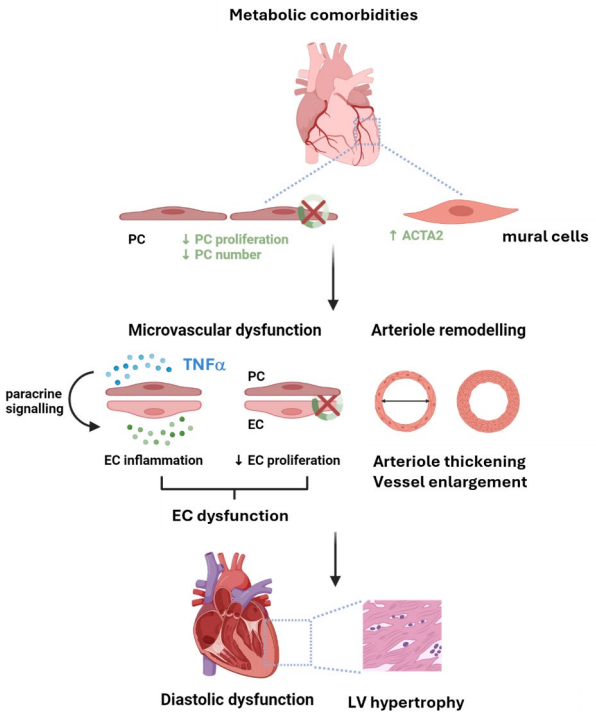

Keywords Pericytes, Smooth muscle cells, Endothelial cells, HFpEF, Diastolic dysfunction

remodelling of the microvasculature, affecting either the endothelial cell (EC) or mural cell compartment. Previous studies have focused mainly on EC dysfunction in HFpEF [4] while the role of mural cells has been overlooked. Pericytes, the mural cells of the capillaries, play an important role in controlling EC biology [5], yet little research has been done on the role of pericytes in the heart and how they communicate with ECs. Pericyte coverage in the murine heart is reduced with aging [6] and recent work from our group showed that pericyte loss precedes the development of diastolic dysfunction in the obese ZSF1 rat HFpEF model [7]. The loss in cardiac pericytes was associated with reduced pericyte proliferation which was seen before the decrease in EC proliferation, and pericytes exposed to oxidative stress sensitised EC to inflammatory signals [7] but whether mural cell dysfunction could play a causal role in EC dysfunction in HFpEF remained to be determined. In this study, we used the diabetic db/db mouse given 1% salt as a new model of HFpEF, to study how mural cell dysfunction contributes to EC and diastolic dysfunction using a combination of histology, single-cell RNA sequencing and NicheNet [8] analysis techniques.

Methods

Experimental mice

BKS.Cg-Dock7m+/+Leprdb/+/J (further referred to as db/+) mice were obtained from Jackson's laboratory (stock no 000700) and bred in house. In the initial experiment, 6-week old db/db mice were given 1% salt in their drinking water for 8 weeks and compared to db/+ mice given 1% salt for 8 weeks, db/db mice without salt treatment (receiving normal drinking water), and db/+ control mice (receiving normal drinking water) For the timeline experiment, 6-week old db/db mice were given 1% salt for 2, 4, 6 and 8 weeks and compared to age-matched littermate db/+ control mice receiving normal drinking water. For the scRNAseq experiment, db/db mice were given 1% salt for 4 weeks. To achieve lineage tracing of mural cells, we intercrossed B6.Cg-Pdgfrbtm1.1(cre/ERT2)Csln/J mice (JAX stock no 030201, further referred to as PDGFRβ-CreERT2) with B6.129 × 1-Gt(ROSA)26Sortm1(EYFP)Cos/J mice (JAX stock no 006148, further referred to as EYFP) [9]. In PDGFRβ-CreERT2$^{tg/tg}$-EYFP$^{tg/tg}$ mice, following tamoxifen injections, EYFP expression is induced only in those cells that express PDGFRβ. PDGFRβ-CreERT2$^{tg/tg}$-EYFP$^{tg/tg}$ were then crossed with db/+ mice to study the behaviour of pericytes during HFpEF. The desired genotypes for our

experiment were: PDGFRβ-CreERT2$^{tg/+}$-EYFP$^{tg/+}$-db/+ and PDGFRβ-CreERT2$^{tg/+}$-EYFP$^{tg/+}$-db/db. Both males and females were used. To activate Cre recombinase, mice were given 100 µl of 10 mg/ml tamoxifen per 10 g BW via intraperitoneal injection for a total of 10 injections (5 days/week, 2 days' rest, 5 days/week), followed by one week of rest. Mice were housed under a 14-hour light 10-hour dark cycle with access to water and chow diet ad libitum (V1534-000, Ssniff Spezialdiäten GmbH).

Genotyping protocols

Ear biopsies were genotyped with the following primers for Leprdb 5'-AGAACGGACACTCTTTGAAGTCT C-3' (forward) and 5'-CATTCAAACCATAGTTTAGGT TTGTGT-3' (reverse) [10]. The following PCR genotyping protocol was used: 94 °C for 5 min, followed by 35 cycles of 94 °C for 30s, 52 °C for 30s and 72 °C for 1 min, with final extension at 72 °C for 10 min. Next, 1 µl of RsaI restriction enzyme (R0167, NEB) was added to the PCR product and incubated at 37 °C for 15 min (no heat inactivation needed). Db/+ show 3 bands (at 135 bp, 108 bp and 27 bp), db/db show 2 bands (at 108 bp and 27 bp) and wildtype mice only 1 band at 135 bp. For PDGFRβ-Cre, the following primers were used: 5'- CCACCTTGAAT GAAGTCAACAC-3' (common), 5'-AGCTTGTGGCAG TGTAGCTG-3' (wildtype reverse, product 272 bp) and 5'-ACATGTCCATCAGGTTCTTGC-3' (mutant reverse, product 320 bp) with the following PCR touchdown protocol: 94 °C for 2 min, followed by 10 cycles of 94 °C for 20s, 65 °C for 15s (with − 0,5 °C decrease per cycle) and 68 °C for 10s, then 28 cycles of 94 °C for 15s, 60 °C for 15s and 72 °C for 10s, with final extension at 72 °C for 2 min. For EYFP, the following primers were used: 5'-CTGGCT TCTGAGGACCG-3' (wildtype forward), 5'-CAGGACA ACGCCCACACA-3' (wildtype reverse, product 142 bp), 5'-AGGGCGAGGAGCTGTTCA-3' (mutant forward) and 5'-TGAAGTCGATGCCCTTCAG-3' (mutant reverse, product 384 bp). Two separate reactions, for the detection of wildtype and mutant bands, were prepared. The PCR protocol is the same as for PDGFRβ-Cre.

Fasting glucose and blood pressure measurements

To assess fasting glucose levels, db/+ and db/db + 1% salt mice were fasted for 6 h, and glucose levels were measured via a tail vein puncture at 2, 4, 6 and 8 weeks. Blood pressure was assessed using the tail cuff method. Seven days before the measurements, the mice were placed in the restrainer to acclimatise. On the day of measurement, 10 cycles were recorded to acclimatise the animal, followed by at least 10 cycles for analysis. The average of these 10 measurements was taken per animal, for both systolic and diastolic blood pressure.

Transthoracic echocardiography

Db/+ and db/db + 1% salt mice were anesthetized using 3% inhaled isoflurane (Ecuphar NV) for induction followed by 1% inhaled isoflurane for maintenance. Transthoracic echocardiography was performed as previously described [7]. In brief, a MX550D transducer (13–24 MHz) connected to a Vevo 3100 echocardiograph (Visual Sonics) was used. Animals were placed on their backs on a heating pad to maintain the body temperature around 37.6°C, measured by a rectal probe. Heart rate (HR), ejection fraction (EF), left ventricular volumes as well as end-diastolic and -systolic volume (EDV and ESV, respectively) were assessed by parasternal short-axis M-mode imaging. Left ventricular filling was assessed by pulsed wave Doppler trans-mitral flow velocity tracings, including early mitral inflow peak velocity I, mitral valve deceleration time (MV DT), isovolumic relaxation time (IVRT) and aortic ejection time (AET) was calculated. Early diastolic mitral annulus peak velocity (E') was measured by tissue Doppler imaging at the lateral mitral annulus. E/E' ratios were calculated. At least three stable cardiac cycles were averaged per animal.

Tissue collection

Db/+ and db/db + 1% salt mice were weighted and anesthetised by intraperitoneal injection of 100 mg/kg ketamine and 10 mg/kg xylazine dissolved in 0.9% NaCl. The hearts of the mice were perfused with PBS before collection. Hearts were weighed and normalised to tibia length (TL). The top part of the heart was fixed in 4% paraformaldehyde at 4 °C for 24 h and embedded in paraffin. Another equally sized section was flash frozen in liquid nitrogen, and later embedded in optimal cutting medium for cryosectioning. Picro Sirius Red staining was performed on paraffin embedded sections (4 µm) to assess fibrosis. The perivascular cardiac fibrosis ratio was quantified as the percentage of Sirius Red positive area per perivascular area. Paraffin embedded sections were also stained for Laminin A (Sigma Aldrich L9393, 1/400) to assess cardiomyocyte hypertrophy. The cardiomyocyte cross-sectional area was calculated based on the inner circumference of at least 100 cardiomyocytes per laminin-stained section (5 images where 20 cardiomyocytes per image were counted; only cardiomyocytes where the nucleus was visible were included). Frozen cardiac tissue (5 µm) sections were stained with Isolectin GS-IB$_4$-488 (IB4, Thermofisher, I21411, 1/100), rabbit neuron glial antigen 2 (NG2, EMD Millipore, Ab5320, 1/100), goat PDGFRβ (R&D, AF1042, 1/50), rabbit Collagen IV (Biorad, 2150 – 1470, 1/400), rabbit Ki-67 (Abcam, ab15580, 1/100), goat VE-Cadherin (R&D, AF1002, 1/50), and α-smooth muscle actin– Cy5 (αSMA, Sigma-Aldrich, C6198, 1/200), chicken anti-GFP (Abcam, 13970) and goat anti-PDGFRα (R&D, AF1062, 1/100))

antibodies. Paraffin sections were stained with IB4 and rabbit anti-p21 antibody (Novus, NB100-1941, 1/50). Anti-rabbit Alexa Fluor 555, anti-goat Alexa Fluor 647 and anti-chicken 488 were used as secondary antibodies (1/500). Pericyte coverage was determined by counting the number of capillary vessels (IB4+) that are covered by NG2 + and PDGFRβ + cells. Capillary vessels are defined as vessels smaller than 10 µm in diameter. 20 µm thick frozen sections were used to evaluate the jaggedness of junctions on a VE-Cadherin staining. 3–5 images were taken per animal and evaluated 'blindly' by an independent observer. The VE-Cadherin junctions were scored as either 'straight' (score 1) or 'jagged' (score 3). Then, the median of all images per animal was calculated. We then counted how many mice were scored 1, 2 or 3. Next, chi square was used to calculate the distribution and its significance per group. For endothelial cell proliferation, we calculated the percentage of vessels with at least one proliferating endothelial cell. For all stainings, 3–5 images were taken per animal. For the ACTA2 staining, one image of the whole heart was taken with the Axioscan 7 (Zeiss). Half of the kidney was fixed in 4% paraformaldehyde at 4 °C for 24 h and embedded in paraffin. Another part of the kidney was kept for qPCR. Paraffin-embedded sections were stained with Picro Sirius Red to assess renal fibrosis. To assess mesangial expansion, we measured the size of 10 glomeruli per kidney per mouse and took the average.

Isolation of single cells from mouse heart

4 male PDGFRβ-CreERT2$^{tg/+}$-EYFP$^{tg/+}$-db/+ and 4 male PDGFRβ-CreERT2$^{tg/+}$-EYFP$^{tg/+}$-db/db hearts were used for the single cell preparation. At the end of the preparation, 4 samples per genotype were pooled into 1 sample. The mouse hearts were flushed with saline, the atria were removed, and the heart was kept in cold PBS and protected from light (i.e. EYFP is light-sensitive). The heart was minced up in a petri dish using a blade under sterile conditions and then transferred into a 15 ml tube with enzyme solution (2.5 mg/ml collagenase I dissolved in PBS containing 20% FBS) for digestion. Samples were incubated at 37 °C for 15-30 min until a single cell suspension was reached. Cells were pipetted up and down to get single cell suspension. Next, cells were passed over a 40 µm cell strainer, washed and spun down at 1500 rpm for 5 min at 4 °C. The supernatant was discarded. Next, cell debris was removed using the cell debris removal kit according to manufacturer's instructions (Miltenyi, 130-109-398). The pellet was resuspended in 2 ml cold red blood cell lysis buffer and incubated for 3 min on ice. After adding cold PBS up to 15 ml and thoroughly mixing, samples were centrifuged at 4 °C at 1000 g for 5 min, washed in PBS, and resuspended in 2 ml FACS buffer (PBS + 0.1% BSA + 2mM EDTA). Then cells were filtered through a 30 µm and 20 µm filter to remove cardiomyocytes. Next, CD45 + cells were depleted using anti-CD45 anti-mouse microbeads (Miltenyi, 130-052-301) and magnetic associated cell sorting (MACS) was performed following the manufacturer's protocol, to enrich for our cell populations of interest (ECs, mural cells, fibroblasts). After washing, samples were re-pelleted by spinning down at 300 g for 5 min 4 °C and resuspended in PBS + 0.04% filtered BSA. Cells were counted using an automated cell counter (Luna FL, Logos Biosystems). The db/+ and db/db sample had a viability of 95% and 93%, respectively. Samples were further diluted to achieve approx. 1×10^6 cells/ml (~ 1000 cells/µl) before loading into 10x Chromium (10x Genomics).

Single cell RNA sequencing

Cells were loaded into 10X Chromium followed by library preparation targeting an average of 10 000 cells per library. All libraries were dual index and prepared using 10 × 3'kit v3.1. Libraries were sequenced at an average depth of 40 000 reads/cells on a Nova seq 6000. Sequencing files were pre-processed using Cell Ranger (10X Genomics) and aligned to the GRCm38 mm10 genome. Data integration, normalisation, clustering, and differential expression analysis were performed using Seurat (version 4.3.0) in R (version 4.2.2). Receptor-ligand interactions were computationally predicted using the R package NicheNet as described in [8]. The following quality control steps were applied: genes expressed by < 3 cells, cells expressing < 150 genes (low quality) or > 4000 RNA features (potential doublets) and > 10% of unique molecular identifiers (UMIs) derived from the mitochondrial genome were removed. Clusters containing contaminating blood cells (*Hbb*) or cardiomyocytes (*TTN*, *DMD*$^+$) were removed from subsequent analysis. The scRNA-seq data set can be found in the Gene Expression Omnibus repository (accession number: GSE263197).

Transmission electron microscopy

Samples were fixed in 4% paraformaldehyde and 2.5% glutaraldehyde in 0.1 M sodium cacodylate buffer, and after washing in the same buffer, subsequently treated with 1% osmium tetroxide and 1.5 mM ferrocyanide in 0.1 M sodium cacodylate buffer. Then, after washing in 0.1 M cacodylate buffer, the samples were stained *en bloc* with 1% uranyl acetate and lead aspartate [11]. Finally, the samples were rinsed and dehydrated in a graded ethanol series from 30 to 100% after which they were washed in propylene oxide and embedded in epoxy resin. Ultrathin Sect. (70 nm) were cut and post-stained in uranyl acetate. The sections were examined, and images taken with a JEOL JEM1400 transmission electron microscope equipped with an 11 Mpxl EMSIS Quemesa camera.

8–10 images were taken per animal blindly by an independent researcher.

Coculture of pericytes and endothelial cells

Immortalized human pericytes from 2 male donors (Celther, CL 05008-CLTH) were cultured in DMEM (Thermofisher, 41965039) supplemented with penicillin/streptomycin and 10% fetal bovine serum. The cells were screened for the expression of canonical markers by qPCR. To mimic oxidative stress (OX), pericytes were stimulated with or without 100 μM H_2O_2 for 24 h. Healthy or OX-treated pericytes were co-cultured with endothelial cells (HUVECs) in transwell inserts in a 24-well plate (Corning, 353095, 0.4 μm pore size) preventing direct cell-cell contact. H_2O_2-treated (or control) pericytes were seeded in the inserts (20,000 cells/insert) and endothelial cells (30,000 cells/well) were seeded on the bottom of the well. Pericytes and endothelial cells were co-cultured for 7 days in endothelial cell-specific medium with one medium change halfway. To knockdown *TNFA*, pericytes were transfected with siRNA against human *TNFA* (ON-TARGETplus® SMART Pool, Dharmacon, L-010546-00-0005) or siControl (ON-TARGETplus® Control Pool, nontargeting pool, Dharmacon, D-001810-10-05) using Lipofectamine RNAiMAX transfection reagent (13778030, Invitrogen). To assess proliferation, endothelial cells were plated on cover slips before the start of the coculture and analysed using the Click-iT EdU kit (C10340, Thermo Fisher Scientific). At day 6 of the coculture, cells were incubated with EdU (10μM) for 24 h. The next day, cells were fixed, permeabilised and incubated with the Click-iT reaction cocktail (containing CuSO4, Alexa fluor 555 azide, reaction buffer and additive) for 30 min protected from light. Next, cells were washed and stained with DAPI for 10 min, and then mounted on glass slides using Prolong Glass Antifade (P36980, Invitrogen). The following day, cells were imaged on a Zeiss widefield microscope, and the number of EdU-positive cells (average taken of 3 fields of view) quantified using ImageJ. Senescence was determined using the Senescence Cells Histochemical Staining Kit (CS0030, Sigma-Aldrich). To avoid a too high degree of confluence (which results in false positive staining), endothelial cells were trypsinised and replated at day 6 of the coculture, at a cell density of 10×10^3 cells in a 24-well plate. The next day, cells were fixed for 7 min at RT, washed and incubated with staining mixture (containing X-gal) overnight at 37 °C. Images were taken using a Zeiss Axio inverted microscope. The percentage of SAβG-positive cells (average taken of 3 fields of view) was quantified using ImageJ.

Real time quantitative polymerase chain reaction (qPCR)

Kidneys were homogenised in Qiazol using ceramic beads. RNA was extracted from the kidney and from cells using the Qiagen Rneasy mini kit (74104). RNA was converted into cDNA using M-MLV reverse transcriptase (Promega, M1701) and oligoDT primers (ThermoFisher, N8080128). Quantitative real-time PCR was performed using SYBR Green PCR master mix (ThermoFisher, 4364344). All primer sequences are listed in Supplemental Table 1. Data were normalised to housekeeping genes RPL13A (human) and HRPT (mouse).

Western blotting

Whole cell protein lysates were prepared in RIPA buffer, supplemented with proteinase inhibitors and phosphatase inhibitors (Thermo Scientific, 78440). Protein concentration was determined using BCA method (23227, Pierce BCA protein assay kit, ThermoFisher). Immunoblotting was performed according to standard conditions, using 7% polyacrylamide gels, methanol-based wet transfer and chemiluminescence detection (32106, Pierce ECL Substrate, ThermoFisher Scientific). The following primary antibodies: P-eNOS (Ser1177) (9571, CST), eNOS (610296, BD), P-STAT1 (Tyr701) (9167, CST), STAT1 (14994, CST) and Cyclin D1 (2978, CST) were used and detected using HRP-labelled secondary antibodies. GAPDH (10R-G109B, Biosynth) was used as loading control.

Statistical analysis

Statistical analysis was performed using GraphPad software V8. Results are presented as mean ± SEM. Data with at least two independent variables were analysed using a two-way ANOVA with Sidak's comparison post-hoc test. Data with two groups were analysed using a two-tailed unpaired Student's t-test or a Mann Whitney U test in case of non-parametric testing. Statistical significance for the scores of jaggedness were analysed with a Pearson chi squared test. Differences between distributions were calculated using Z-statistics. P-values of < 0.05 were considered statistically significant.

Results

Db/db mice develop diastolic dysfunction after 8 weeks of 1% salt

HFpEF strongly associates with metabolic comorbidities such as type-2 diabetes and obesity [2]. We therefore used the diabetic db/db mouse to develop a new mouse model of HFpEF. Db/db mice generally develop hyperglycaemia and obesity at young age [12], but the progression to cardiac dysfunction usually happens later, around 6 months of age [13, 14], and may [15] or may not [16] be associated with hypertension. To get a more robust cardiac phenotype, we treated 6-week-old db/db mice

with 1% salt for 8 weeks. 1% salt intake in mice is considered moderately high for mice and adequately models the effects of high-sodium intake in humans. Db/db + salt mice developed diastolic dysfunction, as evidenced by an increase in E/E' (ratio of early passive filling of the left ventricle to mitral annular velocity (E')), cardiomyocyte hypertrophy, cardiac fibrosis and a preserved ejection fraction, when compared to db/+ controls and db/+ mice given 1% salt (Suppl Fig. 1). Age-matched db/db mice without salt treatment did not show significant signs of diastolic dysfunction at this stage, including no cardiac fibrosis (Suppl Fig. 1). Interestingly, 1% salt treatment did not cause hypertension (Suppl Fig. 1), but kidneys of db/db + salt mice showed increased intraglomerular mesangium size (Suppl Fig. 2), indicating mesangial expansion, one of the key structural changes leading to renal dysfunction in diabetic nephropathy [17]. The mesangial expansion was at least partially due to increased deposition of extracellular matrix, but the degree of fibrosis did not differ between groups (Suppl Fig. 2). Importantly, the 1% salt intake had no effect on the kidneys of the db/+ mice but increased the salt sensitivity of the kidneys of the db/db mice. Based on the absence of an increased blood pressure, and no changes in renal expression of sodium channels such as sodium glucose co-transporter 2 (SGLT2) and epithelial sodium channel (ENaC) (Suppl Fig. 2), we propose that the salt-induced renal dysfunction in the db/db mice promotes diastolic dysfunction through increased volume overload (due to hampered fluid regulation), rather than sodium retention.

Next, we performed a timeline study treating db/db mice with 1% salt for 2, 4, 6 and 8 weeks to explore the time-dependent changes in their metabolic and cardiac phenotype, using the db/+ mice without salt treatment as control. From 6 weeks of age, db/db + salt mice already showed increased body weight and developed hyperglycaemia compared to db/+ mice (Fig. 1A, B). Signs of diastolic dysfunction were only evident in the db/db mice at 8 weeks of salt (Fig. 1C, Supplemental Table 2), which presented with preserved ejection fraction (Fig. 1D). An increase in heart weight at 6 weeks of salt was present (Fig. 1E), whereas cardiomyocyte hypertrophy was already seen as of 4 weeks of salt (Fig. 1F, G). In parallel with the diastolic dysfunction, total fibrosis was only increased from 8 weeks of salt (Fig. 1H, I), but this was not associated with perivascular fibrosis (0.48% ± 0.10 vs. 0.50% ± 0.09 perivascular ratio). Interestingly, the increase in E/E' was more pronounced in the females (Suppl Fig. 3), which is line with the observed sex-differences in patients with HFpEF [18].

Capillary density loss, pericyte loss and vessel regression are all present before the onset of diastolic dysfunction

We next investigated the changes to the microvasculature in relation to the development of diastolic dysfunction. Capillary density, as determined by the number of IB4 + microvessels per area, was reduced in the db/db mice from 6 weeks of salt (Fig. 2A, B). In parallel, we observed a decrease in the number of pericytes (NG2 + and PDGFRb+) per area in db/db mice vs. db/+ mice (Fig. 2B, C). However, when we determine the pericyte coverage, there is no difference between the groups (Fig. 2D). It is therefore unclear whether pericytes are lost because the capillaries regressed, or whether pericyte loss promotes capillary regression. As such, we further investigated active vessel regression defined by the presence of collagen IV^{+} IB4^{-} vessels, so called "empty collagen sleeves". An increase was seen in the db/db mouse heart at 4 and 6 weeks of salt, but no longer at 8 weeks (Fig. 2E, F). Importantly, all these events occurred prior to cardiac dysfunction.

Hearts of db/db + salt mice show signs of endothelial dysfunction and an anti-angiogenic signature

To determine the cellular and molecular mechanisms underlying mural cell dysfunction in HFpEF, we crossed the db/+ mouse with PDGFRβ-CreERT2$^{tg/tg}$-EYFP$^{tg/tg}$ mice to lineage trace the mural cells during HFpEF development (Suppl Fig. 4A). Staining for EYFP and pericyte (PC) markers revealed > 90% recombination efficiency in cardiac pericytes (Suppl Fig. 4B, C). However, the PDGFRβ-CreERT2 also labelled smooth muscle cells (not shown) and therefore we could not use EYFP for pericyte-specific lineage tracing. Nevertheless, no EYFP + NG2-/PDGFRβ- cells were observed, indicating that only cells of the mural cell lineage were EYFP labelled. Because most microvascular changes initiate at 4 weeks of salt, we chose this time point for single-cell RNA sequencing. We used cardiomyocyte-depleted and immune cell-depleted hearts to enrich for vascular cells ($n = 4$ pooled), comparing PDGFRβ-CreERT2$^{tg/+}$-EYFP$^{tg/+}$-db/db + 1% salt to PDGFRβ-CreERT2$^{tg/+}$-EYFP$^{tg/+}$-db/+ mice. We identified 17 clusters from db/+ ($n = 3604$ cells) and db/db + 1% salt ($n = 2741$ cells) mice with 3 major cell types, ECs (Cap1, Cap 2, Cap3_interferon, Cap 4_Sca-1; arteriole, venules, arteries, proliferating and angiogenic), fibroblasts (FB_Pdgfra and Fb_Apoe) and mural cells (VSMC_PC). Endocardium ECs, lymphatic ECs (LEC) and a small population of intracardiac neurons (ICN) were also annotated (Fig. 3A and Suppl Fig. 4D). No differences were observed when clustering per genotype (Fig. 3B). Interestingly, we found that arteriole ECs (expressing markers such as *Cxcl12*, *Rbp7* and weakly positive for *Hey1*, the latter also found in arteries) were increased while the proportion of both angiogenic

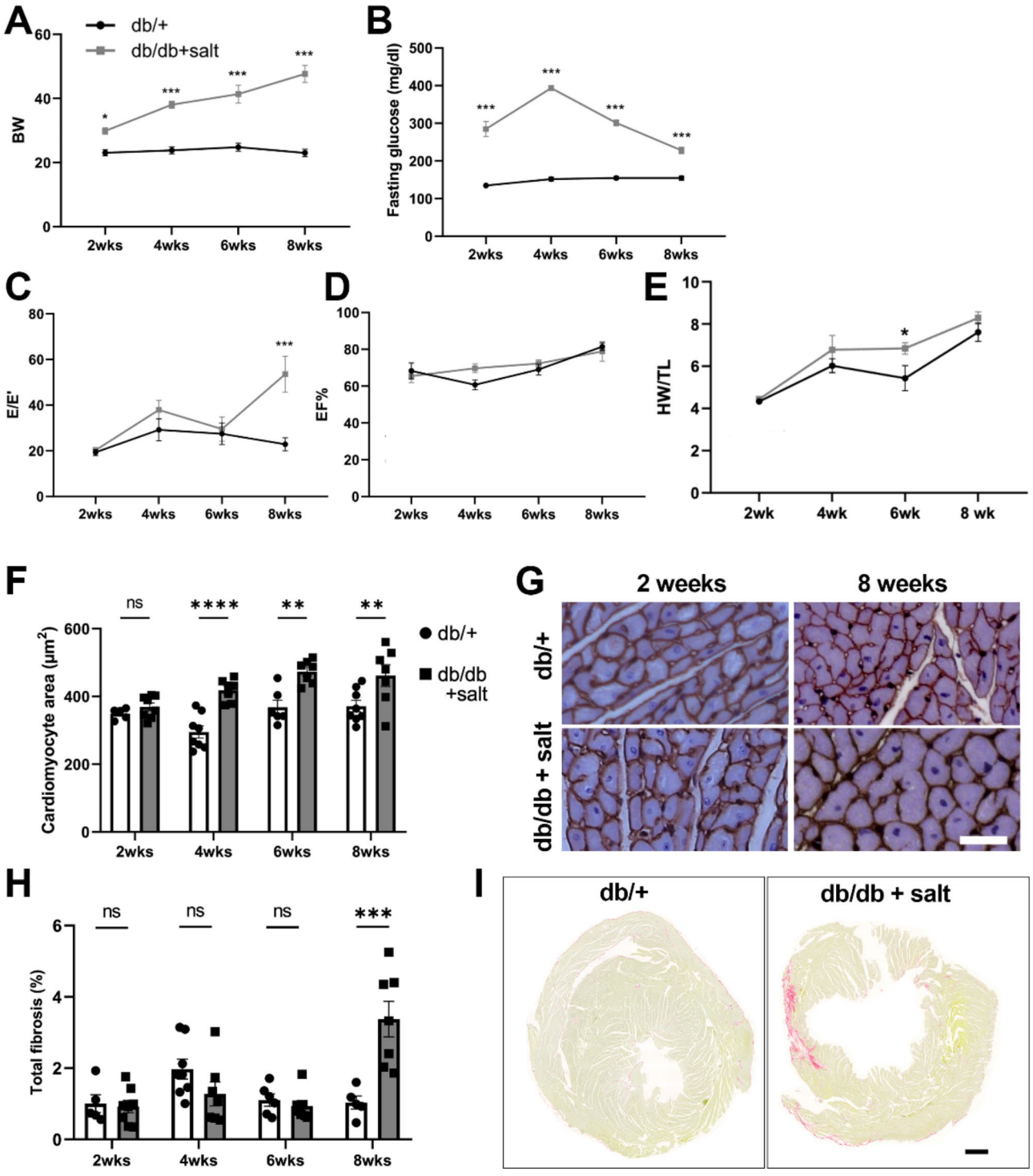

Fig. 1 Db/db mice develop diastolic dysfunction after 8 weeks of 1% salt. (**A**) Body weight, (**B**) fasting glucose, (**C**) E/E' ratio, and (**D**) ejection fraction (EF%) measured by echocardiography in db/+ and db/db + 1% salt mice. (**E**) Heart weight normalised to tibia length (HW/TL). (**F**, **G**) Cardiomyocyte cross-sectional area measured on laminin staining with representative images at 2 and 8 weeks ($n = 5$–8/group) (scalebar is 30 µm). (**H**, **I**) Total fibrosis measured on a Sirius red staining with representative images at 8 weeks ($n = 5$–8/group) (scalebar is 500 µm). Values are presented as mean ± SEM. Two-way ANOVA followed by Sidak's multiple comparisons test with $^{*}p < 0.05$, $^{**}p < 0.01$, and $^{***}p < 0.001$. E, early mitral inflow peak velocity; E', early diastolic annulus peak velocity; EF, ejection fraction; NS, non-significant. At 2 weeks: $n = 8$ F (1 db/+, 7 db/db) and 5 M (4 db/+, 1 db/db); at 4 weeks: $n = 7$ F (4 db/+, 3 db/db) and 8 M (4 db/+, 4db/db); at 6 weeks: $n = 7$ F (3 db/+, 4 db/db) and 6 M (3 db/+, 3 db/db), at 8 weeks: 9 F (6 db/+, 3 db/db) and 6 M (3 db/+ and 3 db/db)

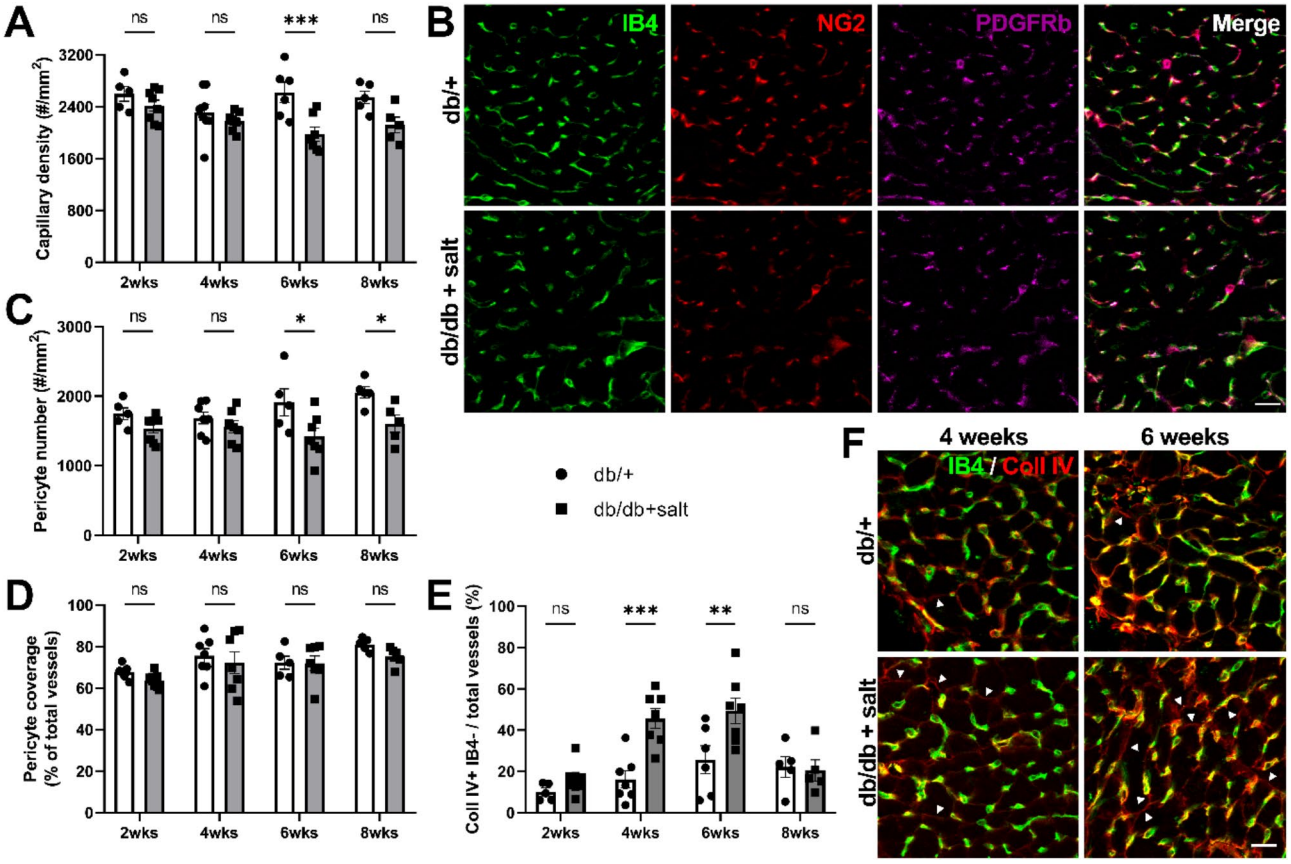

Fig. 2 Db/db mice + 1% salt show microvascular dysfunction before the onset of diastolic dysfunction. (**A**, **B**) Cardiac capillary density measured as the number of IB4 + microvessels per area in db/+ and db/db + 1% salt mice at 2, 4, 6 and 8 weeks with representative images ($n = 5–8$/group). (**C**) Number of pericytes was determined by counting the cells that were double positive for NG2 and PDGFRb marker, and co-localised with IB4 + microvessels. (**D**) Pericyte coverage, assessed by the ratio of IB4 + microvessels covered by NG2/PDGFRb double positive cells over total IB4 + microvessels. (**E**, **F**) Active vessel regression, assessed by the ratio of Coll IV + IB4- microvessels over total IB4 + microvessels with representative images at 4 and 6 weeks ($n = 5–8$/group). White arrowheads indicate empty collagen sleeves. Scalebars are 6 µm. Values are presented as mean ± SEM. Two-way ANOVA followed by Sidak's multiple comparisons test with $*p < 0.05$, $**p < 0.01$, and $***p < 0.001$. IB4, isolectin B4; NG2, neural glial antigen 2; NS, non-significant; PDGFRb, platelet derived growth factor receptor beta; Coll IV, collagen IV. At 2 weeks: $n = 8$ F (1 db/+, 7 db/db) and 5 M (4db/+, 1 db/db); at 4 weeks: $n = 7$ F (4 db/+, 3 db/db) and 8 M (4 db/+, 4db/db); at 6 weeks: $n = 7$ F (3 db/+, 4 db/db) and 6 M (3 db/+, 3 db/db), at 8 weeks: 4 F (2 db/+, 2db/db) and 6 M (3 db/+, 3 db/db)

capillaries (expressing markers of angiogenesis such as *Apln* and *Nrp2*) and proliferating ECs (expressing *Mki67* and *Top2a*) was decreased in the db/db + salt vs. db/+ group (Fig. 3C and Suppl Fig. 4D). GO term analysis on the differentially expressed genes (DEG) of the ECs mostly revealed enrichment of pathways associated with 'EC migration' and 'regulation of angiogenesis' (Fig. 3D), suggesting that the ability of ECs to form new vessels may be altered. Indeed, immunostainings confirmed that db/db + 1% salt hearts are characterised by a reduced percentage of vessels with proliferating ECs (Fig. 3E, F) and abnormal junctional remodelling, determined by an increase in "jagged" VE-Cadherin junctions (Fig. 3G, H).

Hearts of db/db + salt mice show arteriole wall thickening, vessel enlargement, and signs of pericyte detachment

Analysis of the mural cell population for cell-specific marker genes showed that *Pdgfrb* marks all mural cells, although mostly expressed in the PC subcluster compared to the VSMC subcluster (Fig. 4A). The pericyte marker *Kcnj8* was almost exclusively expressed in the PC subcluster whereas the contractile VSMC markers *Myh11* and *Acta2* were exclusively expressed in the VSMC subcluster. Interestingly, the mural cell cluster showed increased expression of *Acta2* and *Myh11* in the db/db + salt compared to db/+ mice (Fig. 4B). GO term analysis on the DEG showed enrichment of pathways associated with 'muscle contraction' among other processes (Fig. 4C). Immunostaining confirmed increased ACTA2 expression in the hearts of db/db mice (Fig. 4D and Suppl Fig. 5A). However, no difference in ACTA2 protein expression was seen in the microvessels nor in the pericytes (Fig. 4E, F and Suppl Fig. 5B). In fact, ACTA2 + vessel density was reduced in db/db + salt hearts compared to controls (Fig. 4G and Suppl Fig. 5A) but the vessel diameter was larger (Z-statistic between

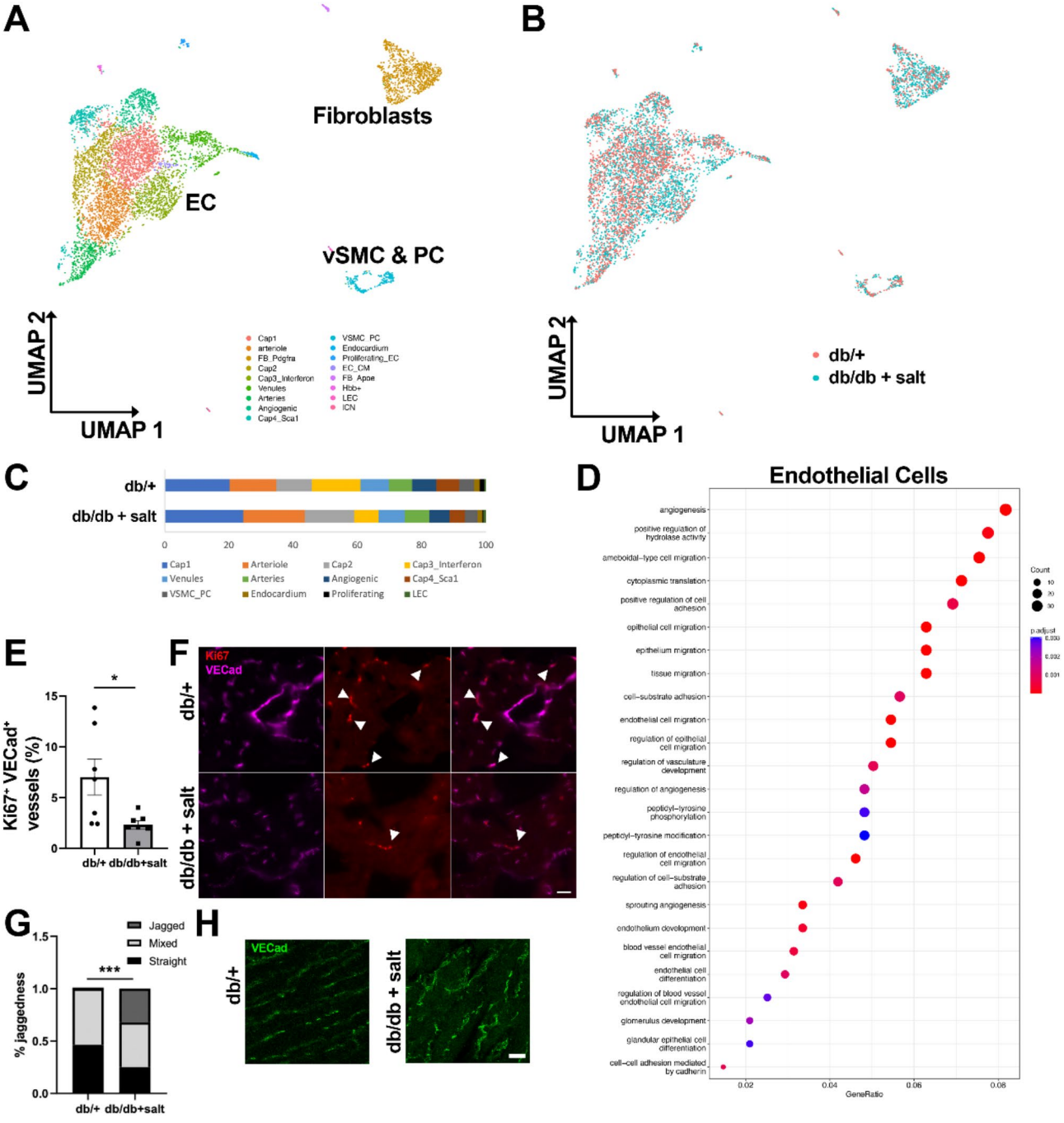

Fig. 3 Hearts of db/db + 1% salt mice show endothelial cell dysfunction and angiogenesis impairment. Single cell analysis on the hearts of PDGFRβ-Cre^{ERT2}-EYFP-db/db mice given 1% salt for 4 weeks and PDGFRβ-Cre^{ERT2}-EYFP-db/+ control mice ($n = 4$ male mice pooled per sample). UMAP showing clustering (**A**) identifying 17 clusters with 3 large cell types (ECs, fibroblasts, and mural cells) or split by genotype (**B**). (**C**) Distribution of cells in PDGFRβ-CreERT2$^{tg/+}$-EYFP$^{tg/+}$-db/+ ($n = 3604$ cells) and PDGFRβ-CreERT2$^{tg/+}$-EYFP$^{tg/+}$-db/db ($n = 2741$ cells) mice shown as percentage of cells. (**D**) GO term analysis (FC = 0.15) on top 500 DEG between PDGFRβ-CreERT2$^{tg/+}$-EYFP$^{tg/+}$-db/+ and PDGFRβ-CreERT2 $^{tg/+}$-EYFP$^{tg/+}$-db/db ECs. (**E**,**F**) Staining for Ki67 to assess EC proliferation with representative images at 4 weeks. White arrowheads indicate proliferating EC (scale bar: 10 µm). (**G**,**H**) Analysis of 'jagged' VE-Cadherin junctions with representative image at 4 weeks (scale bar: 6 µm). Junctions were scored jagged, mixed or straight. All data were analysed by a Student's t-test with $^{*}p < 0.05$, $^{**}p < 0.01$, and $^{***}p < 0.001$ except for data presented in (G) which were analysed by a Pearson's Chi-squared test. VE-Cad, VE-Cadherin

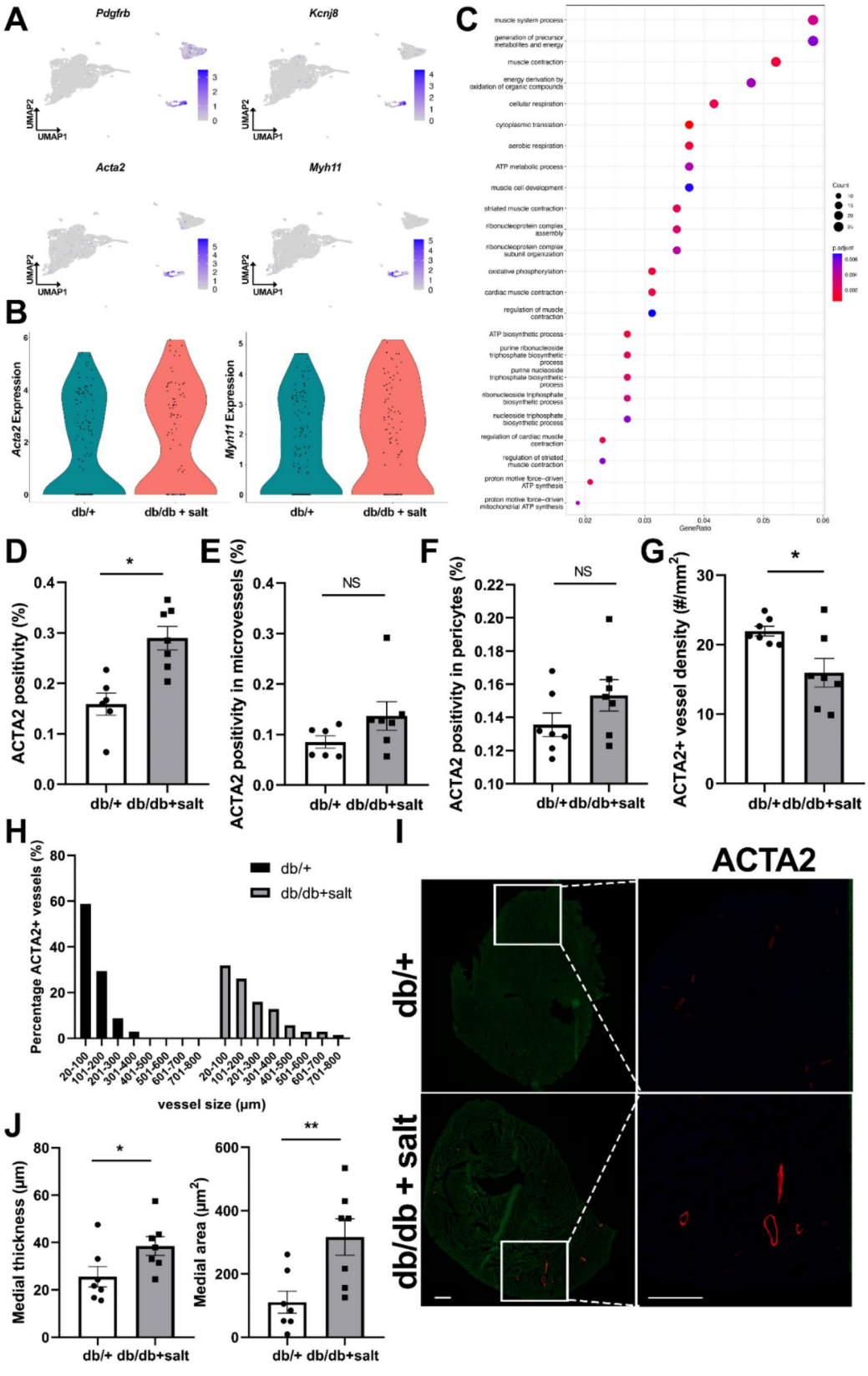

Fig. 4 (See legend on next page.)

(See figure on previous page.)

Fig. 4 Hearts of db/db mice show arteriole thickening and vessel enlargement after 4 weeks of salt treatment. (**A**) Feature plots for *Pdgfrb*, *Kcnj8* (pericyte marker), *Acta2* and *Myh11* (VSMC markers) on single cell data of hearts of PDGFRβ-Cre^{ERT2}-EYFP-db/db + salt and PDGFRβ-Cre^{ERT2}-EYFP-db/+ mice. (**B**) Violin plot of *Acta2* and *Myh11* expression in the mural cell population of db/db + salt vs. db/+ mice. (**C**) GO term analysis on the top 500 DEG of the mural cells (FC = 0.25). (**D**) Percentage of ACTA2 positive area in the hearts of db/+ and db/db + 4-week salt mice. Percentage of ACTA2 positive area in (**E**) microvessels (< 10 µm) and (**F**) cardiac pericytes (identified as double positive for NG2 and PDGFRβ) of db/+ and db/db + 4-week salt mice. (**G**) ACTA2 + vessel density measured as the number of ACTA2 + blood vessels per total heart area. (**H**) Distribution of ACTA2 + blood vessels according to vessel size (µm). (**I**) Representative images of ACTA2 + blood vessels in the hearts of db/+ and db/db + 4-week salt mice. Scale bars: 500 µm. (**J**) Measurement of medial area and medial thickness to assess arteriole thickening. All data were analysed by a Student's t-test with $*p < 0.05$ and $**p < 0.01$ except for data presented in (**H**) which were analysed by Z-statistics to determine a significant difference in distributions. ACTA2, alpha smooth muscle cell actin; NS, non-significant. $n = 7$ F (4 db/+, 3 db/db) and 8 M (4 db/+, 4db/db)

distributions = 6.39) (Fig. 4H, I) and associated with an increase in medial area and medial thickness (Fig. 4J).

This phenomenon of 'arteriolisation' may arise from pericyte transdifferentiating into VSMC-like cells, as described in pulmonary hypertension [19], however, it was impossible to study this because the PDGFRβ-Cre driven EYFP labelling does not distinguish between ACTA2 + pericytes and ACTA2 + VSMCs. Pericytes can also give rise to (myo)fibroblasts, which has been described in kidney fibrosis [20] and upon myocardial infarction [21]. However, we found that less than 1% of YFP + cells in the heart colocalised with the fibroblast marker PDGFRα and there was no difference in the percentage of PDGFRα+/YFP + cells between both groups (Suppl Fig. 5C, D). We therefore have no proof of transdifferentiation of pericytes into fibroblasts, though we also cannot completely exclude this possibility.

Next, we investigated changes in the capillary bed. Db/db mice at 4 weeks of salt showed an increase in the capillary luminal diameter compared to db/+ mice (Fig. 5A, B). Pericyte proliferation was also reduced in db/db + salt vs. db/+ hearts (Fig. 5C, D). We then used TEM to examine the EC-pericyte junctions at the microvessel niche in more detail. Hearts of db/db + salt mice showed a significant increase in the EC-pericyte intercellular area, suggestive of pericyte detachment (Fig. 5E, F). Overall, these early changes at the capillary bed coincide with vessel regression (at 4 weeks of salt) and are seen before capillary density loss (at 6 weeks of salt).

Pericyte dysfunction promotes EC inflammation and EC proliferation arrest through paracrine signalling

To further investigate the interactions between EC and pericytes, we performed NicheNet [8] analysis on the single cell transcriptomic data. Surprisingly, we found little signalling from the ECs to the mural cell population (Fig. 6A). Instead, mural cells signalled strongly to ECs (Fig. 6B). The predicted target genes in the EC population included interferon genes (*Irf1*, *Irf7*), adhesion molecules (*Icam1*, *Vcam1*), chemokines (*Cxcl9*, *Cxcl16*) inflammation-related regulators (*Stat1*, *Nfkbia*) and cell cycle regulators (*Ccnd1*, *Ccnd2*). To study the paracrine effects of pericytes on ECs, we first challenged the pericytes by exposing them to oxidative stress (OX, 24 h) to induce oxidative stress-induced inflammation in the pericytes and then set up a coculture with ECs using transwell inserts. Co-culturing EC with OX-treated pericytes for 7 days led to increased expression of *VCAM1*, *IL1A*, *IL8*, but not *IL6*(Fig. 6C) and no changes in expression of chemokines in ECs (Suppl Fig. 6A). The EC dysfunction was not associated with oxidative stress nor with changes in eNOS signalling (Suppl Fig. 6B, C). Moreover, the ECs co-cultured with OX-treated pericytes upregulated the cell cycle arrest marker p21 (Fig. 6D) and showed reduced proliferation (Fig. 6E). We then assessed if these ECs also undergo cellular senescence but did not find evidence for this (Suppl Fig. 6D). Next, we investigated the expression of targets suggested by the NicheNet analysis, specifically cyclin D1 and STAT1. ECs cocultured with OX-treated pericytes showed reduced protein expression of cyclin D1 and an increase in total STAT1 expression, without changes in STAT1 phosphorylation (Tyr 701) (Fig. 6F). Cytosolic STAT1 has been shown to inhibit the cell cycle by interacting with cyclin D1, thereby promoting its degradation, independent of its tyrosine 701 phosphorylation site [22]. We therefore propose that the growth arrest in the ECs exposed to OX-treated pericytes is mediated through STAT1 downstream signalling. Next, we pursued the role of TNFα herein which was suggested to have the highest regulatory potential among all ligands in the NichetNet analysis. Indeed, OX-treated pericytes upregulated *TNFA* by 20-fold (Fig. 6G) and we previously showed that ECs upregulate *ILA*, *IL8*, *CCL2* and *CXCL1* in response to a low dose of TNFα but only when cocultured with OX-treated pericytes [7], illustrating the ability of dysfunctional pericytes to increase inflammation in ECs in a paracrine manner. In the next set of experiments, we silenced *TNFA* in the pericytes before OX-treatment and repeated the coculture experiments. Knockdown of *TNFA* abolished the increase in *VCAM1* expression in ECs cocultured with OX-treated pericytes (Fig. 6H). Moreover, knockdown of *TNFA* completely rescued the OX-treated pericytes-induced proliferation arrest in ECs (Fig. 6I). These data pinpoint TNFα as a key cytokine in pericyte dysfunction-induced EC growth arrest. In vivo, db/db + salt hearts also showed increased endothelial VCAM1 (Fig. 6J, K) and p21 (Fig. 6L, M) expression.

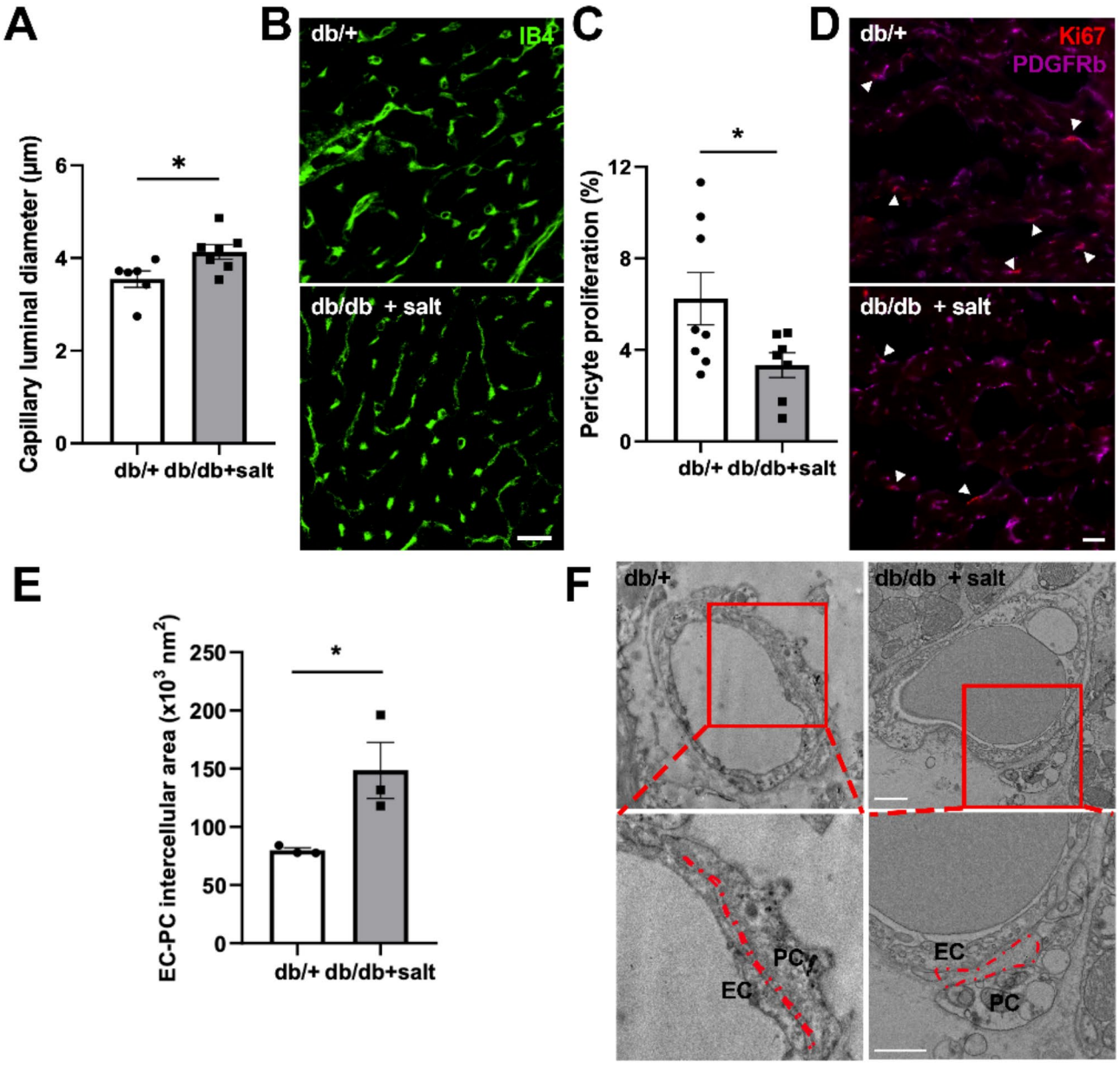

Fig. 5 Hearts of db/db mice show capillary dilatation and increased pericyte-EC intercellular space after 4 weeks of salt treatment. (**A**) Analysis of the capillary luminal diameter in db/db + 4 weeks 1% salt vs. db/+ mice with representative images (**B**). Scale bar: 10 µm. (**C**) Assessment of proliferation of cardiac pericytes (identified by PDGFRβ) by a Ki67 staining ($n = 7–8$/group). White arrowheads indicate proliferating pericytes (**D**). Scale bar: 25 µm. (**E**, **F**) TEM analysis ($n = 3$/group) to determine the intercellular area (E) between EC and pericytes with representative images (**F**). The red dotted line circles the intercellular area. Scale bar: 1 µm

Discussion

We recently showed that pericyte dysfunction precedes diastolic dysfunction in a rat model of HFpEF [7] but whether and how mural cell dysfunction could play a causal and primary role in HFpEF remained unclear. Here, we used diabetic db/db mice given 1% salt, displaying hyperglycaemia, obesity, renal dysfunction and diastolic dysfunction, but not hypertension. As such, we propose a new model of HFpEF in which pressure-independent effects of salt induce renal dysfunction, thereby advancing diastolic dysfunction through volume overload. Indeed, impaired renal function is associated with increased mortality in HFpEF patients but is also a common risk factor and comorbidity and may cause HFpEF possibly through inflammatory and microvascular mechanisms [23]. Of course, our model presents with some limitations as we did not assess other clinical features of HFpEF such as lung congestion, exercise intolerance and vascular stiffness. We further plan to compare our model

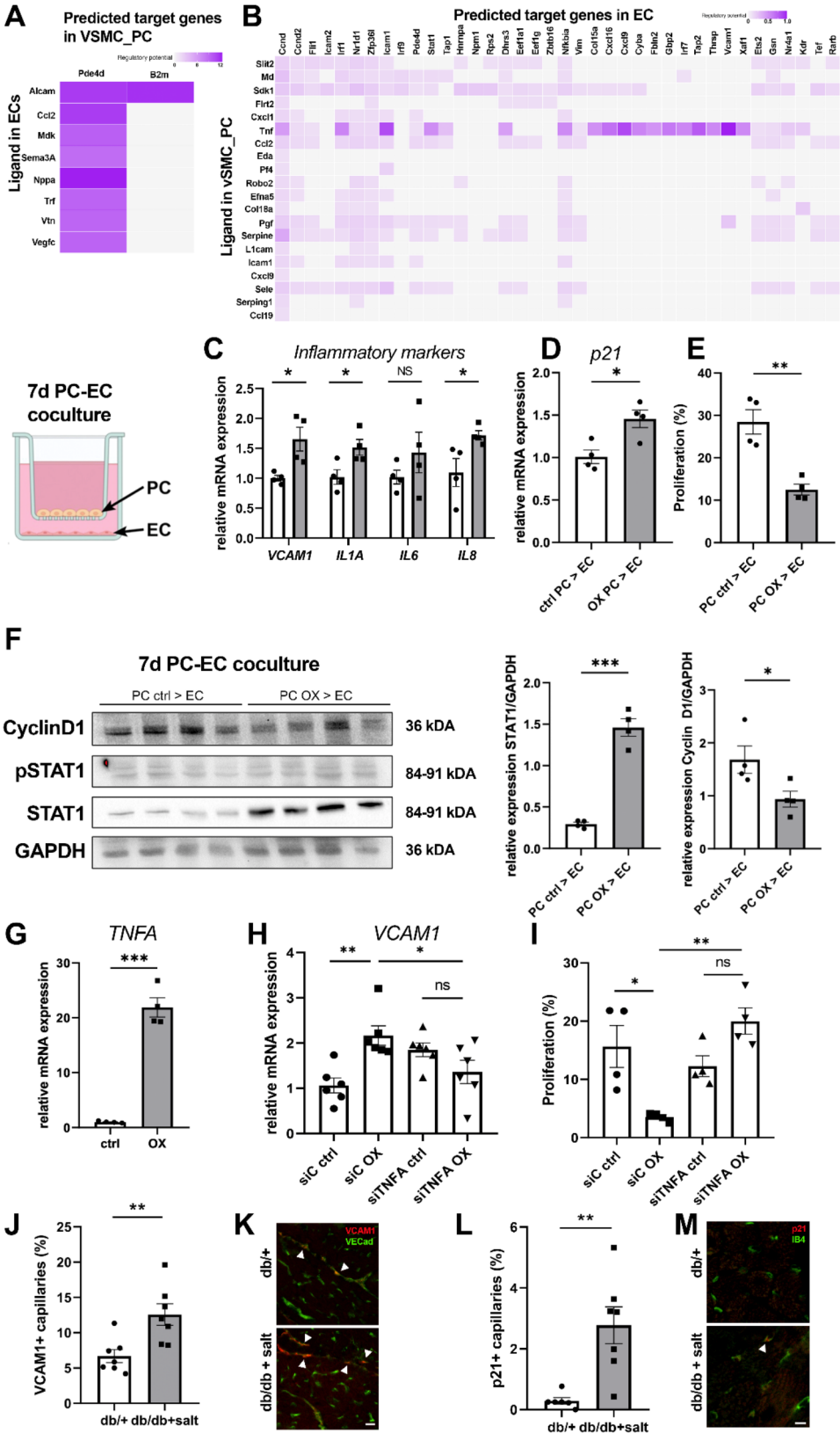

Fig. 6 (See legend on next page.)

(See figure on previous page.)

Fig. 6 Pericyte dysfunction promotes EC inflammation and an EC proliferation arrest through TNFα-dependent paracrine signalling. Predictions of putative ligand-receptor interactions based on NicheNet analysis on the single cell RNA sequencing data between (**A**) the EC (sending) and VSMC_PC (receiver) population and (**B**) the VSMC_PC (sending) population and EC (receiver) population. Human pericytes were exposed to oxidative stress (OX, 100 µM H_2O_2) for 24 h or left untreated (ctrl) and then cocultured for 7 days with ECs. qPCR for (**C**) *VCAM1*, *IL1A*, *IL8 and IL6* and (**D**)*p21* on EC cocultured with healthy or OX-treated pericytes for 7 days. (**E**) Analysis of proliferation by EDU staining. (**F**) Western blot for cyclin D1, P-STAT1 and total STAT1 on EC cocultured with healthy or OX-treated pericytes for 7 days, with quantification. GAPDH was used as loading control. (**G**) qPCR for *TNFA* on pericytes exposed to oxidative stress (OX) for 24 h or left untreated (ctrl). (**H**, **I**) Silencing of *TNFA* in pericytes, followed by OX treatment (or left untreated), and cocultured with ECs for 7 days. qPCR for *VCAM1* (**H**) and analysis of proliferation (**I**) on ECs 7 day cocultured with healthy or OX-treated siTNFA or siCtrl pericytes. All data were analysed by a Student's t-test or One-way ANOVA with $*p < 0.05$, $**p < 0.01$, $***p < 0.001$. IB4, isolectin B4; NS, non-significant; STAT1, signal transducer and activator of transcription 1, TNFA, tumor necrosis factor alpha; VCAM1, vascular adhesion molecule 1. (**J**, **K**) VCAM1 + microvessels (%) in db/+ and db/db + 1% salt mice with representative images at 4 weeks ($n = 7$–8/group). White arrowheads indicate VCAM1 + microvessels (scale bar: 6 µm). (**L**, **M**) p21 + microvessels in db/+ and db/db + 1% salt mice with representative images at 4 weeks ($n = 6$–7/group). White arrowheads indicate endothelial cells positive for p21 (scale bar: 5 µm)

with other models of cardiometabolic HFpEF (e.g. angiotensin II model) in future studies.

Here, in this model of salt-induced renal dysfunction in the db/db mouse, we provide evidence that microvascular dysfunction (i.e. loss of vessel density, vessel regression, pericyte loss, EC dysfunction, capillary dilatation, and pericyte detachment) induces cardiomyocyte hypertrophy, cardiac fibrosis and diastolic dysfunction. Mechanistically, we provide novel insights that endothelial dysfunction, defined as reduced EC proliferation and increased EC inflammation is at least partially initiated by pericyte dysfunction via TNFα-dependent paracrine signalling. At the macrovascular level, we show that coronary intramyocardial vessels undergo arteriole wall thickening and vessel enlargement, preceding the development of diastolic dysfunction. Overall, our findings identify a mechanism by which a pathological mural cell–EC crosstalk induces coronary blood vessel remodelling, both at the microvascular and macrovascular niche, which contributes to the development of HFpEF.

Previous studies indicate a prominent role for EC dysfunction in HFpEF [4]. Our scRNAseq data (i.e. reduced proportion of angiogenic and proliferative ECs in db/db + salt hearts) combined with histology supports a mechanism of reduced angiogenesis whereby ECs emigrate from the regressing vessels. Migration is currently the most well-accepted mechanism for vessel enlargement, a process whereby existing vessels are being reshuffled in response to signals for vascular remodelling [24]. Since db/db + salt mice exhibited fewer but larger arterioles/arteries, we hypothesise vessel enlargement took place, which is well-described in myocardial ischemia [25] and predominantly driven by hemodynamic stress [26]. Our findings are in line with the angiogenesis impairment described in a recent paper from Li et al. where they did scRNAseq on mouse hearts where HFpEF was induced by high fat diet and treatment with the NO inhibitor L-NAME [27]. The same paper showed that the VSMC population was characterised by a highly proliferative and contractive phenotype [27]. The thickening of small arteries and arterioles is also typical for cerebral small vessel disease (cSVD), a disease heavily associated with the same comorbidities that are linked to HFpEF, where it leads to hypoperfusion of the capillary network in the brain [28]. Because it is very difficult to measure perfusion in the capillaries of a mouse heart, we detected an increase in the luminal capillary diameter in the db/db + salt mice vs. db/+ mice, suggestive of capillary dilatation. This has also been described in the brain of mice with an acute [29] or chronic [30] loss of pericytes. The observed increase in capillary luminal diameter, reduced pericyte proliferation and capillary density loss are in line with our previous observations in the obese ZSF1 rat model of diastolic dysfunction [7], suggesting that these early changes in the microvasculature are a common feature of comorbidities-induced HFpEF and are thus not model specific.

The phenomenon of 'arteriolisation' and the increase in cardiac fibrosis in the db/db + salt hearts prompted us to investigate the possibility of pericyte transdifferentiation. Unfortunately, the lack of a specific marker for pericyte lineage tracing made it impossible to study transdifferentiation into myofibroblasts or VSMC-like cells because one cannot distinguish between ACTA2 + pericytes and ACTA2 + VSMCs as they are both EYFP labelled (due to the PDGFRβ-Cre). Although others [6 [21], described that pericyte loss or dysfunction can lead to increased cardiac fibrosis, we do not have solid evidence that pericytes contributed substantially to the fibroblast population in the early phases of diastolic dysfunction.

It is well-accepted that ECs and pericytes communicate to each other, either by direct contact or paracrine signalling [31], but how this communication happens during HFpEF was not known. We predicted potential ligand-receptor interactions with a functional role in HFpEF using NicheNet [8] and to our surprise, we found few signals from the ECs to the mural cells in the heart. Instead, mural cells signalled strongly to the EC compartment. NicheNet suggested a strong interaction between mural cell-derived TNFα and ECs, with inflammatory and cell cycle arrest genes as potential targets. We tested this hypothesis in vitro using a pericyte-EC coculture system and confirmed increased *VCAM1* and interleukins expression, and reduced proliferation in ECs when

exposed to OX-treated pericytes. Knockdown experiments indicated pericyte-derived TNFα as one of the key cytokines driving the EC inflammation and proliferation arrest. Our in vitro findings are in line with the observed increase in endothelial VCAM1 and p21 expression in the db/db + salt hearts and with previous reports showing that pericyte loss leads to upregulation of endothelial adhesion molecules in the lung [32], brain [33] and central nervous system [34]. Pericytes can control EC proliferation and quiescence through either physical contact or secretion of paracrine factors, as described during vessel sprouting [35]. When pericyte function is impaired or lost, vessel remodelling occurs, resulting in either growth or regression of the endothelium, depending on the presence or absence of angiogenic factors [36]. Here, we provide evidence that during the onset of HFpEF, pericyte dysfunction promotes EC inflammation and inhibits EC proliferation through paracrine signalling via TNFα and downstream signalling through STAT1.

Conclusion

Without refuting the current paradigm that endothelial dysfunction plays an important role in microvascular dysfunction in HFpEF, our findings advocate for a prominent and primary role of mural cell dysfunction that occurs prior to microvascular and diastolic dysfunction in HFpEF. Pericyte regulation of endothelial cell biology may be the crucial factor, and the thus far missing link in cardiovascular diseases of chronic inflammation such as HFpEF.

Abbreviations

ACTA2	Alpha smooth muscle actin
AET	Aortic ejection time
CMD	Coronary microvascular dysfunction
DEG	Differentially expressed genes
E	Early mitral inflow peak velocity
EF	Ejection fraction
EDV	End-diastolic volume
EC	Endothelial cell
HFpEF	Heart failure with preserved ejection fraction
IVRT	Isovolumic relaxation time
E'	Mitral annular velocity
MV DT	Mitral valve deceleration time
NG2	Neuron glial antigen 2
OX	Oxidative stress
PDGFRβ	Platelet derived growth factor receptor beta
PC	Pericyte
STAT	Signal transducer and activator of transcription 1
TL	Tibia length
TEM	Transmission electron microscopy
TNFα	Tumour necrosis factor alpha
VCAM1	Vascular cell adhesion molecule 1
VSMC	Vascular smooth muscle cell

Supplementary Information

The online version contains supplementary material available at https://doi.org/10.1186/s12933-025-02623-w.

Supplementary Material 1

Acknowledgements

We would like to thank Prof. P. Herijgers for providing the non-invasive CODA tail-cuff system, and Petra Vandervoort, Mathias Stroobants, Beau Gommers and Sabine Wyns for their assistance in the lab. SH thanks for the support of IMI2-CARDIATEAM (N° 821508). We acknowledge the support from the Netherlands Cardiovascular Research Initiative, an initiative with support of the Dutch Heart Foundation, Dutch Cardiovascular Alliance DCVA- Double Dosis, 2020-B005. The graphical abstract was generated with BioRender.com

Author contributions

M.O.J.G. and E.A.V. designed the project and wrote the paper. E.A.V. was also in charge for the visualisation. E.A.V. and S.H. secured project funding and supervised the work. M.O.J.G. generated data for all figures. A.P. analysed the scRNAseq data and thus generated data for Figs. 3, 4 and 6. J.R. and S.J.S. generated data for Fig. 1 and suppl Fig. 1. B.C. and U.C. generated data for Figs. 4 and 5, respectively. M.D. and P.C. secured funding for the scRNAseq experiment and provided valuable scientific input. All authors read and approved the final manuscript.

Funding

We acknowledge the support of Fonds voor Wetenschappelijk Onderzoek [G0B5920N to EAVJ and SH]. We acknowledge the support from the European Research Area Networks on Cardiovascular Diseases (ERA-CVD) [ENRICH to EAVJ] as well as the support of the European Union's Horizon 2020 research and innovation program through the project CRUCIAL [848109 to EAJV].

Data availability

Data is provided within the manuscript or supplementary information files. The scRNA-seq data set can be found in the Gene Expression Omnibus repository (accession number: GSE263197). Any additional data is available upon request.

Declarations

Ethics approval and consent to participate

All animal experiments were approved by the local ethics committee of KU Leuven (Project 116/2021).

Consent for publication

Not applicable.

Competing interests

SH receives personal fees for independent scientific advice on early development in the field of heart failure from AstraZeneca, Ribocure, and CSL Behring, and receives research support from AstraZeneca and CSL Behring.

Author details

[1]Centre for Molecular and Vascular Biology, Department of Cardiovascular Sciences, KU Leuven, Herestraat 49, box 911, Leuven 3000, Belgium
[2]Endocrinology, Diabetes and Nutrition, UCLouvain, Avenue Hippocrate, box 55, Brussels 1200, Belgium
[3]Laboratory of Angiogenesis and Vascular Metabolism, VIB-KU Leuven Center for Cancer Biology (CCB), KU Leuven, Leuven, Belgium
[4]Center for Biotechnology, Khalifa University, Abu Dhabi, United Arab Emirates
[5]Department of Cardiology, CARIM School for Cardiovascular Diseases, Maastricht University, Universiteitssingel 50, Maastricht 6229 ER, The Netherlands

Received: 18 November 2024 / Accepted: 29 January 2025
Published online: 07 February 2025

References

1. Owan TE, Hodge DO, Herges RM, Jacobsen SJ, Roger VL, Redfield MM. Trends in prevalence and outcome of heart failure with preserved ejection fraction. N Engl J Med. 2006;355(3):251–9.
2. Redfield MM, Borlaug BA. Heart failure with preserved ejection fraction: a review. JAMA. 2023;329(10):827–38.

3. Sinha A, Rahman H, Webb A, Shah AM, Perera D. Untangling the pathophysiologic link between coronary microvascular dysfunction and heart failure with preserved ejection fraction. Eur Heart J. 2021;42(43):4431–41.
4. Paulus WJ, Tschope C. A novel paradigm for heart failure with preserved ejection fraction: comorbidities drive myocardial dysfunction and remodeling through coronary microvascular endothelial inflammation. J Am Coll Cardiol. 2013;62(4):263–71.
5. van Splunder H, Villacampa P, Martinez-Romero A, Graupera M. Pericytes in the disease spotlight. Trends Cell Biol. 2024;34(1):58–71.
6. Tamiato A, Tombor LS, Fischer A, Muhly-Reinholz M, Vanicek LR, Togru BN et al. Age-dependent RGS5 loss in pericytes induces cardiac dysfunction and fibrosis. Circ Res. 2024.
7. Simmonds SJ, Grootaert MOJ, Cuijpers I, Carai P, Geuens N, Herwig M, et al. Pericyte loss initiates microvascular dysfunction in the development of diastolic dysfunction. Eur Heart J Open. 2024;4(1):oead129.
8. Browaeys R, Saelens W, Saeys Y. NicheNet: modeling intercellular communication by linking ligands to target genes. Nat Methods. 2020;17(2):159–62.
9. Srinivas S, Watanabe T, Lin CS, William CM, Tanabe Y, Jessell TM, et al. Cre reporter strains produced by targeted insertion of EYFP and ECFP into the ROSA26 locus. BMC Dev Biol. 2001;1:4.
10. Corem N, Anzi S, Gelb S, Ben-Zvi A. Leptin receptor deficiency induces early, transient and hyperglycaemia-independent blood-brain barrier dysfunction. Sci Rep. 2019;9(1):2884.
11. Walton J. Lead aspartate, an en bloc contrast stain particularly useful for ultrastructural enzymology. J Histochem Cytochem. 1979;27(10):1337–42.
12. Kobayashi K, Forte TM, Taniguchi S, Ishida BY, Oka K, Chan L. The db/db mouse, a model for diabetic dyslipidemia: molecular characterization and effects of Western diet feeding. Metabolism. 2000;49(1):22–31.
13. Mori J, Patel VB, Abo Alrob O, Basu R, Altamimi T, Desaulniers J, et al. Angiotensin 1–7 ameliorates diabetic cardiomyopathy and diastolic dysfunction in db/db mice by reducing lipotoxicity and inflammation. Circ Heart Fail. 2014;7(2):327–39.
14. Alex L, Russo I, Holoborodko V, Frangogiannis NG. Characterization of a mouse model of obesity-related fibrotic cardiomyopathy that recapitulates features of human heart failure with preserved ejection fraction. Am J Physiol Heart Circ Physiol. 2018;315(4):H934–49.
15. Bagi Z, Erdei N, Toth A, Li W, Hintze TH, Koller A, et al. Type 2 diabetic mice have increased arteriolar tone and blood pressure: enhanced release of COX-2-derived constrictor prostaglandins. Arterioscler Thromb Vasc Biol. 2005;25(8):1610–6.
16. Guo C, Martinez-Vasquez D, Mendez GP, Toniolo MF, Yao TM, Oestreicher EM, et al. Mineralocorticoid receptor antagonist reduces renal injury in rodent models of types 1 and 2 diabetes mellitus. Endocrinology. 2006;147(11):5363–73.
17. Steffes MW, Osterby R, Chavers B, Mauer SM. Mesangial expansion as a central mechanism for loss of kidney function in diabetic patients. Diabetes. 1989;38(9):1077–81.
18. Beale AL, Meyer P, Marwick TH, Lam CSP, Kaye DM. Sex differences in cardiovascular pathophysiology: why women are overrepresented in heart failure with preserved ejection fraction. Circulation. 2018;138(2):198–205.
19. Bordenave J, Tu L, Berrebeh N, Thuillet R, Cumont A, Le Vely B, et al. Lineage tracing reveals the dynamic contribution of Pericytes to the blood vessel remodeling in Pulmonary Hypertension. Arterioscler Thromb Vasc Biol. 2020;40(3):766–82.
20. Humphreys BD, Lin SL, Kobayashi A, Hudson TE, Nowlin BT, Bonventre JV, et al. Fate tracing reveals the pericyte and not epithelial origin of myofibroblasts in kidney fibrosis. Am J Pathol. 2010;176(1):85–97.
21. Alex L, Tuleta I, Hernandez SC, Hanna A, Venugopal H, Astorkia M, et al. Cardiac Pericytes acquire a fibrogenic phenotype and contribute to vascular maturation after myocardial infarction. Circulation. 2023;148(11):882–98.
22. Dimco G, Knight RA, Latchman DS, Stephanou A. STAT1 interacts directly with cyclin D1/Cdk4 and mediates cell cycle arrest. Cell Cycle. 2010;9(23):4638–49.
23. Ter Maaten JM, Damman K, Verhaar MC, Paulus WJ, Duncker DJ, Cheng C, et al. Connecting heart failure with preserved ejection fraction and renal dysfunction: the role of endothelial dysfunction and inflammation. Eur J Heart Fail. 2016;18(6):588–98.
24. Gifre-Renom L, Jones EAV. Vessel enlargement in development and pathophysiology. Front Physiol. 2021;12:639645.
25. Buschmann I, Schaper W. The pathophysiology of the collateral circulation (arteriogenesis). J Pathol. 2000;190(3):338–42.
26. Peirce SM, Skalak TC. Microvascular remodeling: a complex continuum spanning angiogenesis to arteriogenesis. Microcirculation. 2003;10(1):99–111.
27. Li G, Zhao H, Cheng Z, Liu J, Li G, Guo Y. Single-cell transcriptomic profiling of heart reveals ANGPTL4 linking fibroblasts and angiogenesis in heart failure with preserved ejection fraction. J Adv Res. 2024.
28. Ohishi M. Hypertension with diabetes mellitus: physiology and pathology. Hypertens Res. 2018;41(6):389–93.
29. Berthiaume AA, Grant RI, McDowell KP, Underly RG, Hartmann DA, Levy M, et al. Dynamic remodeling of Pericytes in vivo maintains capillary coverage in the adult mouse brain. Cell Rep. 2018;22(1):8–16.
30. Hellstrom M, Gerhardt H, Kalen M, Li X, Eriksson U, Wolburg H, et al. Lack of pericytes leads to endothelial hyperplasia and abnormal vascular morphogenesis. J Cell Biol. 2001;153(3):543–53.
31. Gerhardt H, Betsholtz C. Endothelial-pericyte interactions in angiogenesis. Cell Tissue Res. 2003;314(1):15–23.
32. He H, Yang W, Su N, Zhang C, Dai J, Han F et al. Activating NO-sGC crosstalk in the mouse vascular niche promotes vascular integrity and mitigates acute lung injury. J Exp Med. 2023;220(2).
33. Armulik A, Genove G, Mae M, Nisancioglu MH, Wallgard E, Niaudet C, et al. Pericytes regulate the blood-brain barrier. Nature. 2010;468(7323):557–61.
34. Torok O, Schreiner B, Schaffenrath J, Tsai HC, Maheshwari U, Stifter SA et al. Pericytes regulate vascular immune homeostasis in the CNS. Proc Natl Acad Sci USA. 2021;118(10).
35. Eilken HM, Dieguez-Hurtado R, Schmidt I, Nakayama M, Jeong HW, Arf H, et al. Pericytes regulate VEGF-induced endothelial sprouting through VEGFR1. Nat Commun. 2017;8(1):1574.
36. Bergers G, Song S. The role of pericytes in blood-vessel formation and maintenance. Neuro Oncol. 2005;7(4):452–64.

Publisher's note